Experimental and Theoretical Assessment of Protonated Hoogsteen 9-Methylguanine–1-Methylcytosine Base-Pair Dissociation: Kinetics within a Statistical Reaction Framework

SCHOLARONE™
Manuscripts

Experimental and Theoretical Assessment of Protonated Hoogsteen 9-Methylguanine–1-Methylcytosine Base-Pair Dissociation: Kinetics within a Statistical Reaction Framework

May Myat Moe,[ab] Jonathan Benny,[ab] Yan Sun,[ab] and Jianbo Liu*[ab]

[a] Department of Chemistry and Biochemistry, Queens College of the City University of New York, 65-30 Kissena Blvd., Queens, NY 11367, USA; [b] Ph.D. Program in Chemistry, The Graduate Center of the City University of New York, 365 5th Ave., New York, NY 10016, USA

Abstract   We investigated collision-induced dissociation (CID) reactions of protonated Hoogsteen 9-methylguanine−1-methylcytosine base pair (HG-[9MG·1MC + H]$^+$), which is aimed to address the mystery of the literature reported ″anomaly″ in product ion distributions and to compare the kinetics of Hoogsteen base pair with its Waston-Crick isomer WC-[9MG·1MC + H]$^+$ (reported recently by Sun et al.; *PCCP*, 2020, **22**, 24986). Product ion cross sections and branching ratios were measured as a function of center-of-mass collision energy using guided-ion beam tandem mass spectrometry, from which base-pair dissociation energies were determined. Product structures and energetics were assessed using various theories, of which the composite DLPNO-CCSD(T)/aug-cc-pVTZ//ωB97XD/6-311++G(d,p) was adopted as the best-performing method for constructing reaction potential energy surface.   The statistical Rice-Ramsperger-Kassel-Marcus theory was found to provide a useful framework for rationalizing the dominating abundance of $[1MC + H]^+$ over $[9MG + H]^+$ in the fragment ions of HG-[9MG·1MC + H]$^+$. The kinetics analysis proved the necessity of incorporating into kinetics modeling not only the static properties of reaction minima and transition states but more importantly the kinetics of individual base-pair conformers that have formed in collisional activation. The analysis also pinpointed the origin of the statistical kinetics of HG-[9MG·1MC + H]$^+$ vs. the non-statistical behavior of WC-[9MG·1MC + H]$^+$ in terms of their distinctively different intra-base-pair hydrogen-bonds and consequently the missing of proton transfer between the N1 position of 9MG and the N3′ of 1MC in the Hoogsteen base pair. Finally, the Hoogsteen base pair was examined in the presence of a water ligand, i.e., HG-[9MG·1MC + H]$^+$·H$_2$O. Besides the same type of base-pair dissociation as that detected in dry HG-[9MG·1MC + H]$^+$, secondary methanol elimination was observed via a S$_N$2 reaction of water with nucleobase methyl groups.

* E-mail: jianbo.liu@qc.cuny.edu. Tel: 1-718-997-3271.

1. Introduction

The double-helix structure of DNA is built on the hydrogen-bonds (H-bonds) between complementary nucleobases. This complementarity serves as the underlying principle of DNA replication and transcription, which allows cells to copy genetic information from one generation to another and recognize/repair DNA damage. Proton transfer (PT) that occurs along these H-bonds affects the information encoded in the H-bond motif and consequently introduces point spontaneous mutations.[1, 2] Reaction kinetics and dynamics of intra-base-pair PT depend on the base-pair structures and ionization states. In neutral base pairs, PT in one direction prompts another PT in the opposite direction.[1, 3-8] This double PT is, however, not feasible in singly charged base pairs. Instead, single PT becomes prevalent for base pairs in their protonated[9-18] and deprotonated states,[19, 20] radical cations,[3, 21-37] radical anions,[25, 38-42] hydride adducts[14, 43] and metal cation complexes.[44] This results in the formation of two stable conformations for base-pair ions: one adopts a canonical conformation (referred to as a conventional conformer) and the other is produced by intra-base-pair PT (referred to as a PT conformer).

We recently reported a series of experiments as well as molecular dynamics simulations and kinetics modeling of intra-base-pair PT in protonated 9-methylguanine−1-methylcytosine ([9MG·1MC + H]$^+$),[18] deprotonated 9-methylguanine−cytosine ([9MG·C − H]$^-$),[19] deprotonated guanine−cytosine ([G·C − H]$^-$)[19, 20] and 9-methylguanine−1-methylcytosine radical cation ([9MG·1MC]$^{•+}$).[37] These works were focused on the Watson-Crick (WC)[45] isomers of the respective base-pair ions wherein two nucleobases are paired through three H-bonds as illustrated in Scheme 1. In all of these base-pair systems, PT from the guanine N1 position to the cytosine N3′ position (designated as PT1) leads to the interconversion between conventional and PT conformers: WC-[9MG + H$_{N7}$]$^+$·1MC → WC-[9MG + H$_{N7}$ − H$_{N1}$]·[1MC + H$_{N3'}$]$^+$ (reaction enthalpy ΔH = 15.4 kJ/mol), WC-9MG·[C − H$_{N1'}$]$^-$ → WC-[9MG − H$_{N1}$]$^-$·[C − H$_{N1'}$ + H$_{N3'}$] (ΔH = -1.9 kJ/mol), WC-G·[C − H$_{N1'}$]$^-$ → WC-[G − H$_{N1}$]$^-$·[C − H$_{N1'}$ + H$_{N3'}$] (ΔH = -2.9 kJ/mol), and WC-9MG$^{•+}$·1MC → WC-[9MG − H$_{N1}$]$^•$·[1MC + H$_{N3'}$]$^+$ (ΔH = 4.8 kJ/mol). In view of the low activation barrier (8.7 − 17.4 kJ/mol) for PT1 and the similar energies between the conventional and PT conformers

in each reaction system, both conformers should be populated in thermal and collisional activation of the base pairs. We were able to distinguish the conventional vs. PT conformers using collision-induced dissociation (CID) tandem mass spectrometry (MS/MS), wherein the base-pair ions collided with inert gas atoms and produced different dissociation product pairs depending on the dissociating base-pair structures. In case of WC-[9MG·1MC + H]$^+$, the conventional conformer WC-[9MG + H$_{N7}$]$^+$·1MC dissociated into [9MG + H$_{N7}$]$^+$ and neutral 1MC whereas the PT conformer WC-[9MG + H$_{N7}$ − H$_{N1}$]·[1MC + H$_{N3'}$]$^+$ dissociated into neutral [9MG + H$_{N7}$ − H$_{N1}$] and [1MC + H$_{N3'}$]$^+$. Surprisingly, all of these base pairs have presented non-statistical dissociation behavior. The dissociation products of the PT conformers were detected in a higher abundance than those of the conventional conformers regardless of relative energies and populations between the PT and conventional conformers in thermal equilibrium. Quantitatively, the product branching deviated from a statistical product distribution by an order of magnitude or more. These findings have raised the question whether non-statistical dissociation is a systematic feature of all base pairs or a peculiarity due to the WC H-bonding.

Of the various ionization states of the guanine–cytosine (G·C) base pair, protonation has received considerable attention[9-12, 14, 16, 46-49] not only because of its connection with DNA damage and repair but also because of the proton-induced formation of Hoogsteen (HG)[50-54] pairing in addition to WC. The two base-pairing structures are compared in Scheme 1. The conversion from WC to HG requires flipping guanine from an *anti*- to a *syn*- conformation along the N9-bond. The HG base pair retains only the WC H-bond between guanine O6 and cytosine N4′-H but forms a new, ionic H-bond between N7 of guanine and N3′-H of protonated cytosine.[52, 53] Al-Hashimi and co-workers discovered that the protonated WC guanine–cytosine can transiently undergo excursion toward its HG counterpart.[55, 56] The WC-HG interconversion occurs across diverse sequence and position contexts in duplex DNA,[57] and correlates with base-pair opening.[58] Under physiological conditions (pH = 7), 0.01% of G·C may appear as HG-[G·C + H]$^+$.[59] The HG base pair expands the structural and functional complexity and versatility of duplex DNA.[54] For example, the HG guanine–cytosine pair is involved in the formation of a triple helix

between poly(dG)-poly(dC) and ploy (rC) under acidic conditions,[46, 60] and the formation of certain DNA-antibiotic[53] and DNA-protein complexes.[55, 61] HG base pairing also provides a structural motif to pair guanine with cytosine when the guanine WC-edge is damaged,[62] and to replicate both damaged and undamaged DNA.[63, 64] Viewing the different protonation sites (i.e., guanine N7-H in the WC pair vs. cytosine N3′-H in HG), one may presume that PT3′ of HG-G·$[C + H_{N3'}]^+ \rightleftharpoons$ HG-$[G + H_{N7}]^+$·C acts as a prerequisite for the back transition from HG to WC. In this context, the intra-base-pair PT in the HG guanine−cytosine pair is of high biological significance.

Han and co-workers examined the PT and dissociation of HG-$[G·C + H]^+$ by using CID ion-trap mass spectrometry.[13,17] They reported an ″anomalous″ dissociation that resulted in $\frac{[C + H]^+}{[G + H]^+} = \frac{5.5}{4.5}$ in fragment ions,[13] which seemed to contradict the product branching anticipated on the basis of nucleobase proton affinities (PAs). According to the order of $PA(G_{N7}$, protonation at N7$) > PA(C_{O2'}) > PA(C_{N3'})$, $[G + H]^+$ was expected to yield more abundantly in the dissociation of a proton-bound complex.[17] To rationalize the higher $[C + H]^+$ abundance, they proposed intra-base-pair PT3′ and PT7 (see Scheme 1) which result in three dissociating base-pair structures. Two of these produce $[C + H]^+$ (protonated at N3′ and O2′, respectively), and the remaining one produces $[G + H_{N7}]^+$.[17] This was expected to double the formation rate of $[C + H]^+$. Later, the same group compared the CID of HG-[1-methylguanine (1MG)·1MC + H]$^+$ and HG-[9MG·1MC + H]$^{+}$.[65] The first system produced a branching ratio of $\frac{[1MC + H]^+}{[1MG + H]^+} = \frac{4}{1}$ whereas the latter produced $\frac{[1MC + H]^+}{[9MG + H]^+} = \frac{2}{3}$. The alternated product ion abundances were explained by the computational predication that $9MG_{N7}$ has the highest PA, followed by $PA(1MC_{O2'}) > PA(1MG_{N7}) \geq PA(1MC_{N3'})$. But the product branching ratios were far beyond what could be explained by the differences in nucleobase PAs. Particularly, the product branching of HG-$[9MG·1MC + H]^+$ is in striking contrast to HG-$[G·C + H]^+$, despite the similar structures and reaction potential energy surfaces (PESs) of HG-$[9MG·1MC + H]^+$ and HG-$[G·C + H]^+$ and the same order in the PAs of constituent nucleobases. Recently, Cheng et al. argued that product ion branching does not solely depend on nucleobase PAs;

otherwise, the abundance of $[1MC + H]^+$ would be no more than 10% in the CID of HG-$[9MG \cdot 1MC + H]^+$. They introduced two new factors into base-pair dissociation kinetics modeling: a strong ion-induced dipole interaction between N3′-protonated cytosine and polarizable neutral guanine; and an continuously increasing barrier for PT3′ as the base pair begins to dissociate.[66] However, this interpretation led to another extreme that no protonated guanine should be produced at all.

Inspired by the intriguing and evolving research on HG guanine–cytosine, we wish to provide a comprehensive understanding of this system through new measurements and analysis. Note that protonated guanine-cytosine base pairs were generated by electrospray ionization (ESI) of an acidic solution of guanine and cytosine. According to the spectral results of differential ion mobility (DIMS) and infrared multiphoton dissociation (IRMPD),[15] ESI of an acidic base-pair solution produced protonated HG and WC base pairs in a 2:1 ratio. Therefore, Han et al′s CID results of HG-$[G \cdot C + H]^+$ and HG-$[9MG \cdot 1MC + H]^+$ (without isomer separation) represented a mixed contributions from both HG and WC isomers.[13, 65] Using DIMS for isomer separation, Cruz-Ortiz et al.[15] were able to determine isomer-specific product ratio $\frac{[C + H]^+}{[G + H]^+} = \frac{2}{1}$ and $\frac{10}{1}$ for CID of HG- and WC-$[G \cdot C + H]^+$, respectively. We have recently measured the CID of WC-$[9MG \cdot 1MC + H]^+$.[18] Capitalizing on that work, we were able to subtract the WC contribution in the isomer mixture of $[9MG \cdot 1MC + H]^+$ and determined the unbiased CID cross sections and product branching of HG-$[9MG \cdot 1MC + H]^+$. Moreover, the guided-ion-beam techniques utilized in this work allowed us to measure base-pair dissociation under a stringent single ion-molecule collision condition and well-defined collision energy, from which dissociation thresholds and energy dependence were unequivocally determined. All of these have rendered it possible to piece together a more accurate description of base-pair PT and dissociation kinetics and their dependence on the HG- vs. WC-base pair structures.

2. Experiment and Computation

2.1 Guided-Ion-Beam Tandem Mass Spectrometry and CID Measurement

Dissociation thresholds and product ion cross sections of protonated base pairs were measured using a

guided-ion-beam tandem mass spectrometer built at Queens College.[19, 67] The instrument consists of an

ESI ion source, a radio-frequency (rf) hexapole ion guide, a quadrupole mass filter, an rf octopole ion

guide surrounded by a scattering cell, a second quadrupole mass filter and an electron-multiplier ion

detector. 9MG and 1MC were used as prototypes of nucleosides.[18, 37] Gaseous protonated base pairs

were formed by ESI of a methanol/water (3:1) solution containing 0.5 mM 9MG (Chemodex, > 98%) and

0.5 mM 1MC (Enamine, 95%) to the ambient atmosphere (rate 0.06 mL/h) through an electrospray needle

biased at 2.5 kV relative to ground. The positively charged fine droplets were transmitted into the mass

spectrometer through a desolvation capillary (which was heated to 136 °C and biased at 126 V with

respect to ground), and converted to gaseous ions in the source chamber. A 1.0 mm-orifice skimmer is

located at 3 mm away from the end of the capillary, separating the source chamber and the hexapole ion

guide. The skimmer was biased at 24 V relative to ground. The electrical field between the capillary and

the skimmer introduced collision-induced desolvation to remove residual solvent molecules from ions.

Under mild heating and collisions, both dry and monohydrated base-pair ions were produced. Ions

emerging from the skimmer were directed into the hexapole ion guide where ions were thermalized to 310

K by collisions with the background gas at 25 mτ.[67] Ions were then focused into the first quadrupole

mass filter for selection of $[9MG \cdot 1MC + H]^+$ (or $[9MG \cdot 1MC + H]^+ \cdot H_2O$). Ion intensities were 5×10^5

cps for $[9MG \cdot 1MC + H]^+$ and 1×10^4 cps for $[9MG \cdot 1MC + H]^+ \cdot H_2O$, with an initial kinetic energy (KE)

of 0.7 eV and an energy spread (FWHM) of 0.6 eV.

 The $[9MG \cdot 1MC + H]^+$ (or $[9MG \cdot 1MC + H]^+ \cdot H_2O$) ions were injected into the octopole ion guide that

passes through a 10-cm scattering cell, wherein the ions were scattered by Xe (Spectral Gases, 99.995%)

or Ar (T.W. Smith, > 99.5%). The gas pressure was maintained at 0.01 mτ to ensure that base pairs

underwent at most single collisions with the target gas. In addition to providing ion trapping potential in

the radial direction, the octopole was biased at a DC potential. The DC offset was used to control the ion

kinetic energy in the laboratory frame (E_{lab}), thereby setting collision energy (E_{col}) between ions and

collision gas in the center-of-mass frame, that is $E_{col} = E_{lab} \times m_{neutral}/(m_{ion} + m_{neutral})$ where $m_{neutral}$ and m_{ion}

are the masses of collision gas and ions, respectively. After passing the scattering cell, fragment ions and

the remaining reactant ions were mass analyzed by the second quadrupole and counted by the electron

multiplier. Product ion cross sections were calculated from the ratios of reactant and product ion

intensities, the collision gas pressure and the effective length of the scattering cell.

   The compositions of gas-phase base-pair structures depended on the pH of the ESI solution.[15, 66] A

solution of pH 5.8 generated WC-[9MG·1MC + H]$^+$ predominantly (91%) whereas that of pH 3.2

generated a mixture of HG-[9MG·1MC + H]$^+$ (66%) and WC-[9MG·1MC + H]$^+$ (34%).[49] We have

carried out the CID experiment using ESI solutions of pH 3.2 (this work) and 5.8 (in ref 18), respectively.

The two sets of data were used to compute individual cross sections for HG- and WC-[9MG·1MC + H]$^+$.

2.2 Dissociation Threshold Analysis

   CID cross sections were analyzed using a modified line-of-centers (LOC) model.[68-71] For each

dissociation channel, a "true" cross section $\sigma(E_{col}) = \sigma_0 \frac{(E_{col} + E_{vib} + E_{rot} - E_0)^n}{E_{col}}$ was assumed where σ_0 is

an energy-independent scaling factor, E_{vib} and E_{rot} are reactant vibrational and rotational energies, E_0 is

the dissociation threshold, and n is an adjustable parameter that describes the deposition of E_{col} and thus

controls the slope of $\sigma(E_{col})$. The model requires that, at the energies near E_0, at least some of the

collisions are completely inelastic so that E_{col} is all converted to internal energy. This was verified in the

threshold CID of WC-[9MG·1MC + H]$^+$, WC-[9MG·C − H]$^-$, WC-[9MG·1MC]$^{•+}$ and other ions.[18,19, 37, 70]

   $\sigma(E_{col})$ was convoluted with the motion of the neutral (i.e., Doppler broadening) and the rovibrational

states and KE distribution of the ionic reactant. To this end, a Monte Carlo simulation program[37, 72] was

used to sample collision gas with a Maxwell-Boltzmann velocity distribution at 300 K and [9MG·1MC +

H]$^+$ ion beam with a KE distribution of 0.7 eV and vibrational and rotational temperatures at 310 K.

100000 ion-molecule collisions were simulated for each E_{col}. The resulting distributions of the gas

velocities, and the ion KE, E_{vib} and E_{rot} were sampled into the cross section fitting.

   To account for the kinetic shift[73] that occurred when the base-pair dissociation lifetime became

comparable to the instrumental time available for observing reaction, the Rice-Ramsperger-Kassel-

Marcus (RRKM, see below)[74] theory was utilized to determine whether each above-threshold collision led

to detectable dissociation within the ion time-of-flight throughout the mass spectrometer (~500 μs). A

leveling-off collision energy was set so that $\sigma(E_{col})$ reached a plateau at high E_{col}. The rising curvature of

$\sigma(E_{col})$ depends sensitively on E_0 and n. Their values were adjusted until the convoluted $\sigma(E_{col})$ reached

the best agreement with experiment. The uncertainty in E_0 fit was estimated from the range of E_0 values

determined using different sets of n, σ_0 and leveling-off energy.

2.3 Kinetics Modeling Based on Potential Energy Diagram

The global minimum and other important low-energy conformations of HG-[9MG·1MC + H]$^+$ were

calculated at the ωB97XD/6-311++G(d,p) level of theory using Gaussian 09.[75] The range-separated

ωB97XD[76] functional was able to capture short- and long-range interactions, mitigated self-interaction

errors and improved the orbital descriptions of ionic reactants.[34] Basis set superposition errors (BSSEs)[77]

are less than 0.05 eV, and thereby have no influence on the order of stability of various conformers.

Reaction coordinates and potential energy diagram of HG-[9MG·1MC + H]$^+$ were initiated at its

global minimum, both in the absence and the presence of a water ligand. Structures of reaction

intermediates, transition states (TSs) and products formed along the reaction coordinates were optimized

at ωB97XD/6-311++G(d,p). Each TS was verified by intrinsic reaction coordinate calculation that it

connects the reactant with the correct product minimum.

Electronic energies of the ωB97XD/6-311++G(d,p)-optimized structures were refined at ωB97XD/

aug-cc-pVQZ, B3LYP/aug-cc-pVQZ 6-311++G(d,p), the resolution-of-the-identity second-order Møller-

Plesset perturbation theory RI-MP2/aug-cc-pVQZ (which provides accurate description of H-bonds),[78, 79]

and the domain based local pair-natural orbital coupled-cluster single-, double- and perturbative triple-

excitations method DLPNO-CCSD(T)/aug-cc-pVTZ (which serves as a benchmark for base-pair

energies).[80] Calculations at these levels were accomplished using ORCA 4.0.1.[81] Reaction ΔH reported

at each level is based on the sum of electronic energy at the specified level and 298 K thermal correction

at ωB97XD/6-311++G(d,p) (including zero-point energy which was scaled by a factor 0.975[82]).

Following the completion of reaction potential diagram, the RRKM theory[74] was used to predict

dissociation rate and product branching. RRKM assumes that energy is randomized and distributed

among all of the energetically accessible states,[83, 84] and reaction follows the path of least energy on the

PES.[85] The microcanonical rate constant was calculated as $k_{diss}(E,J) = \dfrac{d\sum_{K=-J}^{J} G[E - E_0 - E_r^{\dagger}(J,K)]}{h \quad \sum_{K=-J}^{J} N[E - E_r(J,K)]}$, where G

is the total number of accessible states at TS, N is the density of states in energized reactant, E is the

system energy, E_0 is the dissociation threshold, E_r and $E_r^{\dagger}$ are the rotational energies of the reactant and

the TS, respectively, $E - E_0 - E_r^{\dagger}$(J, K) is the energy that remains once the barrier has been surmounted, J

is the total angular momentum quantum number, d is the reaction path degeneracy, and h is the Planck

constant. Calculations were carried out using the Zhu and Hase version of the RRKM program,[86] in

which N was calculated using Beyer and Swinehart's direct-count algorithm.[87] The values of J, E_0,

vibrational frequencies and moments of inertia for the reactant and the TS were obtained from the

DLPNO-CCSD(T)/aug-cc-pVTZ //ωB97XD/6-311++G(d,p) calculations. J is an adiabatic invariant,

whereas all (2J + 1) K-levels were treated as active to allow energy exchange between vibration and

rotation.[88]

3. Results and Discussion

3.1 HG-9MG·[1MC + H$_{N3'}$]$^{+}$·(H$_2$O)$_{0,1}$ are the Dominating HG Structures

Guided by literature,[11, 15-17, 46, 47, 49, 65, 66] we have identified four low-energy conformers for HG-

[9MG·1MC + H]$^{+}$ that lie within 0.5 eV (48.2 kJ/mol) in energy as presented in Fig. 1. Their Cartesian

coordinates are listed in the Supporting Information. The global minimum conformer pairs 9MG with

protonated [1MC + H$_{N3'}$] via O6···H–N4′ and N7···H^{+}–N3′ and is referred to as HG-9MG·[1MC + H$_{N3'}$]$^{+}$

henceforth. According to the relative energies of different conformers, HG-9MG·[1MC + H$_{N3'}$]$^{+}$ accounts

for > 98% of the HG base-pair population. The second lowest-energy conformer is formed by PT3′ from

N3′ in 1MC to N7 in 9MG, and hence referred to as HG-[9MG + H$_{N7}$]$^{+}$·1MC. HG-[9MG + H$_{N7}$]$^{+}$·1MC

lies in energy 0.10 eV (9.6 kJ/mol) above HG-9MG·[1MC + H$_{N3'}$]$^{+}$ and has only less than 2% population

in the thermodynamical ensemble. The next two HG conformers differ with the first two in that the 9MG

moiety adopts an enol conformation. Both conformers are ~ 0.5 eV (48.2 kJ/mol) higher in energy than

HG-9MG·[1MC + $H_{N3'}$]$^+$ and thus unlikely to be populated in the primary ion beam. A reverse HG

structure[66] was not considered, as its formation was ruled out by the IRMPD spectrum of HG base pair.[15]

Trial geometries for monohydrated base pairs were obtained by adding a water to all of the possible

hydration sites in HG-9MG·[1MC + $H_{N3'}$]$^+$, and then optimized at ωB97XD/6-311++G(d,p). The

converged structures are also illustrated in Fig. 1, in the order of relative ΔH (with regard to the global

minimum) and hydration enthalpy (ΔH$_{hydration}$ = ΔH$_{hydrate}$ − ΔH$_{dry\ ion}$ − ΔH$_{water}$) at 298 K. Their Cartesian

coordinates are provided in the Supporting Information. HG-[9MG·1MC + H]$^+$ presents similar

hydration sites at 1MC as those in WC-[9MG·1MC + H]$^+$,[18] but its 9MG moiety provides the opposite

edge for hydration than its WC-counterpart. The lowest-energy monohydrate, HG-[9MG·1MC +

H]·H_2O_1, has a water bound to N1-H and N2-H in 9MG with ΔH$_{hydration}$ of -0.55 eV (-53.1 kJ/mol). It

has a > 90% population and thus is designated as the representative structure for HG-9MG·[1MC +

$H_{N3'}$]$^+$·H_2O. Some monohydrates, e.g., HG-[9MG·1MC + H]$^+$·H_2O_6, 8 and 9, are formed by charge-

dipole interaction and thus have low ΔH$_{hydration}$. We have also calculated the monohydrates formed at HG-

[9MG + H_{N7}]$^+$·1MC. Even the most stable monohydrate of HG-[9MG + H_{N7}]$^+$·1MC is 0.1 eV (9.6 kJ/mol)

higher in energy than HG-9MG·[1MC + $H_{N3'}$]$^+$·H_2O and therefore insignificant in the ion beam.

In the following data interpretation, the HG-9MG·[1MC + $H_{N3'}$]$^+$ and HG-9MG·[1MC + $H_{N3'}$]$^+$·H_2O

conformers are used as the starting reactants.

3.2 CID of HG-9MG·[1MC + $H_{N3'}$]$^+$

3.2.1 Dissociation Thresholds, and Product Ions, Cross Sections and Branching Ratios

HG-9MG·[1MC + $H_{N3'}$]$^+$ + Xe Isomer-specific CID results were calculated from the two sets of CID

experiments which contained different ratios of HG and WC isomers in the primary ion beam. A

representative dissociation product ion mass spectrum for HG-9MG·[1MC + $H_{N3'}$]$^+$ is shown in Fig. 2a.

Product ions include [9MG + H]$^+$ (*m/z* = 166) and [1MC + H]$^+$ (*m/z* = 126), implying that the PT

conformer HG-[9MG + H$_{N7}$]$^+$·1MC was formed in the collisional activation of HG-9MG·[1MC + H$_{N3'}$]$^+$.

Cross sections for [9MG + H]$^+$ and [1MC + H]$^+$ were measured over an E_{col} range of 0.05 − 6 eV. The

results are plotted in Figs. 2b and c, in which error bars were determined from the four sets of

measurements under the same conditions. The blue-colored lines in the figure are the LOC-model-based

$\sigma(E_{col})$ fit to the experimental data, taking into account energy broadening and kinetic shift. The best fits

are E_0 = 1.85 ± 0.05 eV and n = 2 for dissociation to [9MG + H]$^+$ + 1MC, and E_0 = 1.90 ± 0.05 eV and n

= 1.1 for dissociation to [1MC + H]$^+$ + 9MG. The experimental cross section for [9MG + H]$^+$ appears to

in line with the LOC fit until E_{col} = 3.6 eV; afterwards it starts to decrease due to the competition between
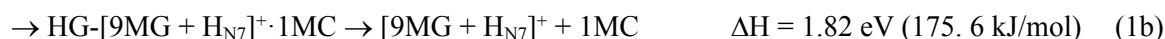
the two product ion pathways.

　　The product cross sections have shown that the abundance of [1MC + H]$^+$ is much higher than that of

[9MG + H]$^+$. The branching ratio of $\frac{[1MC + H]^+}{[9MG + H]^+}$ was plotted as a function of E_{col} in Fig. 2d. The ratio is

near 1.9 at E_{col} = 3.0 eV and rises up to 2.6 at 4.0 eV, indicating that more [1MC + H]$^+$ was formed with

increasing E_{col}. Our detected product ion branching is opposite to that in HG-9MG·[1MC + H$_{N3'}$]$^+$ + He

reported by Han *et al.*[65] The latter was measured under multiple collisions with He gas in an ion trap

without distinguishing WC- and HG-isomers, and the resulting [1MC + H]$^+$ product ion was always less

abundant than [9MG + H]$^+$ with $\frac{[1MC + H]^+}{[9MG + H]^+} = \frac{2}{3}$ at high collision energies. Besides the different

experimental conditions, we note that He-induced collisions are much more impulsive.[89] All of these

factors could have contributed to the different product branching ratios in the two studies. Because

collision energies in Han et al′s experiment were set in an arbitrary instrument unit and only product

formation yields were measured, no dissociation thresholds or product ion cross sections were reported.

HG-9MG·[1MC + H$_{N3'}$]$^+$ + Ar To verify the high [1MC + H]$^+$ abundance observed in the Xe CID, we

repeated the CID experiment using Ar as the target gas. The Ar-induced CID product cross sections and

branching ratios are presented in Fig. 3. Again, [1MC + H]$^+$ has more abundance than that of [9MG +

H]$^+$ throughout the whole E_{col} range, with $\frac{[1MC + H]^+}{[9MG + H]^+}$ being 1.5 at E_{col} = 3.0 eV and 3.0 at E_{col} = 5.0 eV.

Since Ar is lighter, less polarizable and consequently a less efficient collision partner than Xe,[70, 90, 91] it would not prompt CID until E_{col} far exceeds the dissociation threshold.[37, 71, 92] This could be comprehended by comparing the appearance energies of product ions in the Xe- vs Ar-CID in Figs. 2 and 3. For this reason, we did not attempt to extract the E_0 values in the Ar CID or perform He CID (as He is the most impulsive collider).

3.2.2 PES along Intra-Base-Pair PT and Base-Pair Dissociation

Fig. 4 presents various reaction pathways that may occur following the collisional activation of the primary reactant ion HG-9MG·[1MC + $H_{N3'}$]$^+$. These include PT3′ leading to the formation of HG-[9MG + H_{N7}]$^+$·1MC via TS_PT3′ and subsequent PT7 leading to the formation of HG-9MG·[1MC+ $H_{O2'}$]$^+$ via TS_PT7, and the dissociations of the three base-pair conformers as described by reactions (1a – 1c). No isomerization between HG and WC base pairs was considered in collisional activation, as it involves a large nuclear rearrangement and is much slower than dissociation.[15]

HG-9MG·[1MC + $H_{N3'}$]$^+$

$\rightarrow$ 9MG + [1MC + $H_{N3'}$]$^+$ ΔH = 1.86 eV (179. 5 kJ/mol)   (1a)

$\rightarrow$ HG-[9MG + H_{N7}]$^+$·1MC $\rightarrow$ [9MG + H_{N7}]$^+$ + 1MC ΔH = 1.82 eV (175. 6 kJ/mol)   (1b)

$\rightarrow$ HG-9MG·[1MC + $H_{O2'}$]$^+$ $\rightarrow$ 9MG + [1MC + $H_{O2'}$]$^+$ ΔH = 1.81 eV (174. 6 kJ/mol)   (1c)

Reaction enthalpies were compared at ωB97XD/6-311++G(d,p), ωB97XD/aug-cc-pVQZ, B3LYP/ aug-cc-pVQZ, RI-MP2/aug-cc-pVTZ and DLPNO-CCSD(T)/aug-cc-pVTZ. The data are compiled in Table 1. We adopted an energy unit of eV in this work, so that the calculated energetics may be directly compared to the ion-beam experiment. For convenience, we have also listed energies in kJ/mol within parentheses. An excellent agreement was observed among different theories, except that the B3LYP functional constantly underestimated dissociation energies. The DLPNO-CCSD(T)/aug-cc-pVTZ results represent the most accurate calculation, and they best match the experimental dissociation energies. Both TS_PT3′ and TS_PT7 have small activation barriers and presented proton tunneling.[1] The Wigner′s correcting term for quantum mechanical tunneling is $\frac{1}{24}(\frac{h|\nu|}{kT})^2 = 0.6$,[93] where ν is the imaginary frequency

associated with PT. Moreover, the barriers for PT have vanished (i.e., shift to energies below the

resulting PT conformers) after including thermal corrections. All of these have facilitated fast formation

of HG-[9MG + H_{N7}]$^+$·1MC and HG-9MG·[1MC + $H_{O2'}$]$^+$.

Among the three dissociation pathways, reaction (1a) is the mechanistically most straightforward but

bears a slightly higher threshold; reactions (1b) and (1c), on the other hand, are slightly more

energetically favorable but involving consecutive PTs. Note that the thresholds of reactions (1a) and (1c)

differ by only 0.05 eV, so we were not able to distinguish the two in the cross section measurement.

Our calculated potential energy diagram follows the same reaction coordinates as those reported by

Han *et al.*[65] The dissociation energies calculated at DLPNO-CCSD(T)/aug-cc-pVTZ are on average 0.15

eV (14.5 kJ/mol) higher than the results calculated at B3LYP/6-311++G(2d,2p), but very close to those at

CBS-QB3 (within 0.05 eV or 4.8 kJ/mol).[65]

3.2.3 Interpretation of Reaction Outcomes in a Statistical Framework: Tight- and Loose-TS Limits

Han *et al.* interpreted the He-induced CID product branching of HG-9MG·[1MC + $H_{N3'}$]$^+$ in terms of

Cook's kinetics method,[94] i.e., $ln\left(\frac{[1MC\ +\ H]^+}{[9MG\ +\ H]^+}\right) = ln\left(\frac{k_{diss\_[1MC\ +\ H]^+}}{k_{diss\_[9MG\ +\ H]^+}}\right) \approx \frac{PA(1MC) - PA(9MG)}{RT}$, where

$k_{diss\_[1MC\ +\ H]^+}$ and $k_{diss\_[9MG\ +\ H]^+}$ represent the dissociation rates of a proton-bound base pair to the

constituent ions [1MC + H]$^+$ and [9MG + H]$^+$, respectively; and PAs are as defined before.[65] The entropy

effect accompanying the structural rearrangement was ignored due to rigid planar reaction structures.

They predicted [1MC + $H_{N3'}$]$^+$: [1MC + $H_{O2'}$]$^+$: [9MG + H_{N7}]$^+$ = 0.06 : 0.35 : 1. However, the relative

populations of HG-9MG·[1MC + $H_{N3'}$]$^+$ and its two PT conformers (HG-9MG·[1MC + $H_{O2'}$]$^+$ and HG-

9MG·[1MC + H_{N7}]$^+$) were not considered in the model. Neither were the dissociation rate constants of

the individual conformers. Also, the branching ratio was predicted using a thermal equilibria ensemble at

300 K which did not reflect collisional excitation and effective internal temperature of the base pair.

In order to take into account both thermodynamical and kinetics factors, we have evaluated individual

product ion branching ratios in the Xe CID using $\frac{N_i(E) \times k_{diss.i}(E,J)}{\sum N_i(E) \times k_{diss.i}(E,J)}$. N_i represents the density of states for

each energized base-pair conformer that has formed in the collisional activation. At E_{col} above the dissociation threshold, interconversions between different conformers are facile. Therefore, N_i for each conformer is determined by its formation ΔH and reflects its population. The dissociation rate constant k_{diss} for each conformer was calculated using the RRKM theory. Since there is no reverse barrier (i.e., no saddle point) for base-pair dissociation, TS was assumed for dissociation in two hypothetical reaction scenarios.[73, 95-98] In one scenario with a so-called ″tight″ TS, vibrational frequencies of the TS are adopted from those of the dissociating base pair with the removal of the symmetric stretching frequency of the intra-base-pair H-bonds as the latter corresponds to the dissociation reaction coordinate (RC). In the other scenario with a ″loose″ TS, all of the base-pair frequencies that are partitioned into products and thus present little changes upon dissociation (i.e., conserved modes[99]) are preserved in the TS. Of the remaining 6 translational modes[99] which are lost upon dissociation: the symmetric stretching of the intra-base-pair H-bonds is removed; and the other five modes (i.e., out-of-plane twisting, out-of-plane butterfly bending, anti-symmetric out-of-plane bending/step, in-plane bending/gearing and anti-symmetric stretching of the two bases with respect to one another) become intermolecular motions and their frequencies are scaled to account for TS looseness and dissociation entropy. The sum of TS states is very sensitive to the scaling factor for the translational modes. A factor of 0.5 was used in this work, following the statistical treatment of weakly bonded complexes.[18, 37, 95-97] Properties of loose TSs are provided in the Supporting Information.

As suggested by one of the reviewers, we tested orbiting TSs[73] for base-pair dissoication. A orbiting TS is a loose association of the products located at the centrifugal barrier and the translational modes in the TS all convert to rotations of fragement species, i.e., TS has 3N(total number of reactant atoms) − 12 vibrations from the products, 8 rotations (a 2D external rotor, a 1D external rotor and 5 internal rotors), 3 translations and the RC. However, the orbiting TS-based k_{diss} was found to be much slower compared to the experimental ion detection time. Therefore, orbiting TS was not adopted in base-pair kinetics analysis (note that intermolecular interaction is more strong in a dissociating base pair than in a typical ion-

molecule complex[37]).

Reactions were evaluated as a function of E_{col} from 2.2 to 4.2 eV. This is the region where collisions occurred above the dissociation thresholds and energy transfer followed the LOC model. The results are summarized in Table 2. It can be seen that HG-9MG·[1MC + $H_{N3'}$]$^+$ has a dominating population at all of the collision energies. Formation of HG-[9MG + H_{N7}]$^+$·1MC is significant and its population approaches that of HG-9MG·[1MC + $H_{N3'}$]$^+$ at high E_{col}, whereas formation of HG-9MG·[1MC + $H_{O2'}$]$^+$ remains minor with its population $\leq$ 3% throughout the whole range of E_{col}.

The contribution of each conformer to dissociation products depends on not only its population but also its dissociation rate constant. The latter was evaluated on the basis of tight- and loose-TSs, respectively. In both tight- and loose-TS scenarios, HG-9MG·[1MC + $H_{O2'}$]$^+$ dissociates most quickly, followed by HG-[9MG + H_{N7}]$^+$·1MC (which is 1 − 3 orders of magnitude slower than HG-9MG·[1MC + $H_{O2'}$]$^+$) and then HG-9MG·[1MC + $H_{N3'}$]$^+$ (which is 2 − 4 orders of magnitude slower than HG-9MG·[1MC + $H_{O2'}$]$^+$). As a consequence, the fast dissociation rate of HG-9MG·[1MC + $H_{O2'}$]$^+$ outweighs its low population. The population-weighted product branching ratios are compared in the 3rd and 4th columns in the Table, each of which was based on the tight- and loose-TSs, respectively. Qualitatively, both tight- and loose-TS-RRKM have predicted that the dissociation products are dominated by [1MC + H]$^+$ (of which [1MC + $H_{O2'}$]$^+$ is the main composition whereas [1MC + $H_{N3'}$]$^+$ accounts for no more than 20%). Thus from the kinetic analysis, we have an answer in regards to the dominant dissociation pathways and product structures. Quantitatively, the loose-TS-RRKM has predicted a higher $\frac{[1MC + H]^+}{[9MG + H]^+}$ ratio than the tight-TS-RRKM. As there are some low-frequency vibrational modes in a base pair and 5 translational modes in a loose TS, the harmonic oscillator approximation may be problematic in the evaluation of complex density of states and TS sum of states. To this end, anharmonic corrections were made by the method of Haarhoff.[100] It turned out that the anharmonic corrections greatly increased the density of states of all base-pair conformers (more prominent with increasing E_{col}), and the extent of increment is in the order of HG-9MG·[1MC + $H_{N3'}$]$^+$ < HG-[9MG + H_{N7}]$^+$·1MC < HG-9MG·[1MC +

$H_{O2'}]^+$. It follows that the relative populations of HG-[9MG + $H_{N7}]^+ \cdot$1MC and HG-9MG$\cdot$[1MC + $H_{O2'}]^+$

have increased moderately. On the other hand, the dissociation rate constants of all three conformers

have decreased to a similar extent (i.e., reduced by ~60%) with the anharmonic corrections. As a result,

the anharmonic loose-TS-RRKM has predicted slightly higher ratios of $\frac{[1MC\ +\ H]^+}{[9MG\ +\ H]^+}$ (increase by 25% at

high energies) than the harmonic model. Both harmonic and anharmonic models have produced similar

E_{col} dependence of product branching. Therefore, the effects of low frequencies have largely cancelled

out in the statistical product branching calculations.

A more stringent test for kinetics modeling is to compare its product branching ratios with the

experimental observables. Since we were not able to distinguish [1MC + $H_{O2'}]^+$ vs. [1MC + $H_{N3'}]^+$ in the

mass spectra, their intensities are lumped together in Fig. 2d. On the one hand, the RRKM prediction

agrees well with the experiment as far as the major product channel is concerned. Indeed, both tight- and

loose-TS-RRKM models (the RRKM results shown in Fig. 2d are based on the harmonic oscillator model)

are able to predict the dominance of [1MC + H]$^+$ in the experiment. However, neither of the two RRKM

models are able to reproduce the exact product ion abundances in the experiment. In fact, the

experimental branching ratios fall within the range between the tight- and loose-TS predictions. This

implies that the properties of one or more base-pair dissociation TSs are between these two limits and

varies with E_{col}, being tight near the dissociation threshold and becoming loose with increasing E_{col}. This

is contrary to an usual expectation that TS is getting close to reactant structure as internal energy

increases.[94]

3.2.4 Ion-Dipole Effect

One assumption implicit in the statistical kinetics is no recrossing of TS, i.e., once the dissociating

base pair crosses a TS, it does not turn around to recombine.[83] However, the chance for a reversal is

expected to become large for reactions without reverse barriers. On the basis of kinetics modeling, Cheng

et al. suggested that, above dissociation threshold, the lifetime of excited HG base pair must be long

enough that multiple instances of intra-base-pair H-bond lengthening and contracting may be possible.[66]

Assuming that the recombination of separating nucleobases is governed by ion-molecule capture, we may

describe the base-pair recombination rate constant as $k = 2\pi q(\alpha/\mu)^{\frac{1}{2}} + 0.386 \times 2\pi q\mu_D(\frac{2}{\pi\mu kT})^{1/2}$,[101] where

α and μ_D denote respectively the polarizability and permanent dipole moment of the neutral nucleobase, q

is the ion charge, and μ is the reduced mass of the base pair. The first term in k describes the Langevin

rate due to charge-induced dipole,[102] and the second term represents the average ion-neutral capture due

to the permanent dipole.[103, 104]

According to the ωB97XD/6-311++G(d,p) calculations, 9MG has α of 16.07 Å³ and μ_D of 7.18 D,

and 1MC has α of 12.60 Å³ and μ_D of 6.41 D. The calculated ion-neutral capture rate constant for 9MG +

[1MC + H]⁺ is 13% higher than that for 1MC + [9MG + H]⁺, which may lead to the decreasing of [1MC +

H]⁺ abundance in product ions. But this effect is not sufficient to account for the difference between the

experimental value and the loose-TS-RRKM prediction at low E_{col}.

3.2.5 Comparison with WC-[9MG·1MC + H]⁺

It is informative to compare the CID of HG-[9MG·1MC + H]⁺ with that of its WC-counterpart which

we have reported recently.[18] In the latter case, CID is mediated by four base-pair conformers that have

formed in collisional activation:

WC-[9MG + H$_{N7}$]⁺·1MC

→ [9MG + H$_{N7}$]⁺ + 1MC	ΔH = 1.65 eV (159.2 kJ/mol)	(2a)
→ WC-[9MG + H$_{O6}$]⁺·1MC → [9MG + H$_{O6}$]⁺ + 1MC	ΔH = 1.90 eV (183.3 kJ/mol)	(2b)

→ WC-[9MG + H$_{N7}$ − H$_{N1}$]·[1MC + H$_{N3'}$]⁺ → [9MG + H$_{N7}$ − H$_{N1}$] + [1MC + H$_{N3'}$]⁺

ΔH = 2.50 eV (241.2 kJ/mol)　　　(2c)

→ WC-[9MG + H$_{O6}$ − H$_{N1}$]·[1MC + H$_{N3'}$]⁺ → [9MG + H$_{O6}$ − H$_{N1}$] + [1MC + H$_{N3'}$]⁺

ΔH = 1.70 eV (164.0 kJ/mol)　　　(2d)
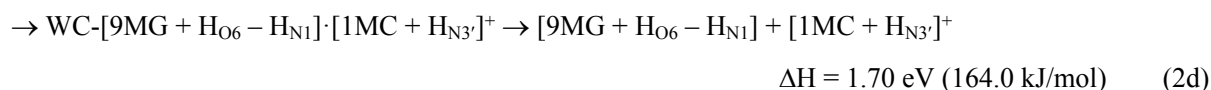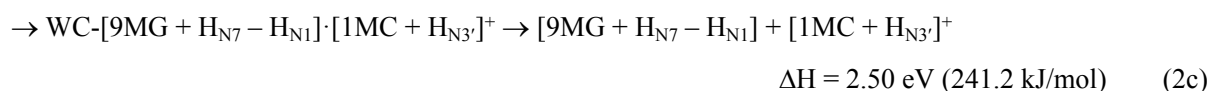
Similar to HG-[9MG·1MC + H]⁺, the CID product ions of WC-[9MG·1MC + H]⁺ were dominated by

[1MC + H]⁺. The ratio of $\frac{[1MC + H]^+}{[9MG + H]^+}$ increases with increasing E_{col}, contrary to a statistical prediction.

However, assuming that reaction (2c, PT1) adopts a more loose dissociation TS (i.e., using a smaller

scaling factor 0.25 for the translational modes in the TS) than reactions (2a, b and d), we were able to

reproduce product ion branching ratios and their E_{col}-dependence. Therefore, the origin of the non-statistical unimolecular kinetics of WC-$[9MG + H_{N7}]^+ \cdot 1MC$ can be linked to the faster dissociation of a particular conformer WC-$[9MG + H_{N7} - H_{N1}] \cdot [1MC + H_{N3'}]^+$.
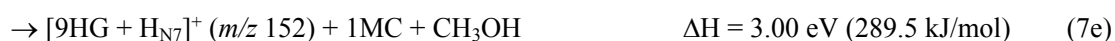
Following the same idea, we have attempted to model reactions (1a − c) of HG-$[9MG \cdot 1MC + H]^+$ by choosing different TS-looseness for different pathways. However, it turned out to be not possible to reproduce the experimental product branching of HG-$[9MG \cdot 1MC + H]^+$ by only adjusting TS properties empirically. This implies that there may be additional, dynamics factors that govern the CID of HG-$[9MG \cdot 1MC + H]^+$. Among these, an obvious factor is the missing of an intra-base-pair H-bond between the N7-H of 9MG and the N3′ of 1MC and consequently PT1 in HG-$[9MG \cdot 1MC + H]^+$.

3.3 Reactions of HG-9MG·$[1MC + H_{N3'}]^+ \cdot H_2O$

3.3.1 More Products Are Produced Due to Base-Pair Monohydration

After completing the study of dry HG-9MG·$[1MC + H_{N3'}]^+$, we proceeded to the collision-induced reactions of its monohydrate. A representative Xe-induced CID product ion mass spectrum for HG-9MG·$[1MC + H_{N3'}]^+ \cdot H_2O$ is shown in Fig. 5a. Many new product ions were detected. Their assignments, possible reaction pathways and reaction enthalpies are listed below, except those of m/z 144 (i.e., $[1HC + H]^+ \cdot CH_3OH$), 158 ($[1MC + H]^+ \cdot CH_3OH$), 184 ($[9HG + H]^+ \cdot CH_3OH$) and 190 ($[1MC + H]^+ \cdot (CH_3OH)_2$). All of the latter are attributed to the secondary reactions of $[1MC + H]^+$, $[1HC + H]^+$ and $[9HG + H]^+$ with methanol and thus were lumped into the corresponding primary products.

HG-9MG·$[1MC + H_{N3'}]^+ \cdot H_2O$

→ HG-9MG·$[1MC + H_{N3'}]^+$ (m/z 291) + H_2O	$\Delta H = 0.47$ eV (45.3 kJ/mol)	(3a)
→ HG-$[9MG + H_{N7}]^+ \cdot 1MC$ (m/z 291) + H_2O	$\Delta H = 0.58$ eV (56.0 kJ/mol)	(3b)
→ HG-9MG·$[1MC + H_{O2'}]^+$ (m/z 291) + H_2O	$\Delta H = 0.79$ eV (76.2 kJ/mol)	(3c)
→ $[9MG + H_{N7}]^+$ (m/z 166) + 1MC + H_2O	$\Delta H = 2.29$ eV (221.0 kJ/mol)	(4)
→ $[1MC + H_{N3'}]^+$ (m/z 126) + 9MG + H_2O	$\Delta H = 2.33$ eV (224.8 kJ/mol)	(5a)
→ $[1MC + H_{O2'}]^+$ (m/z 126) + 9MG + H_2O	$\Delta H = 2.28$ eV (220.0 kJ/mol)	(5b)
→ HG-9MG·$[1HC + H_{N3'}]^+$ (m/z 277) + CH_3OH	$\Delta H = 1.04$ eV (100.3 kJ/mol)	(6a)
→ HG-$[9MG + H_{N7}]^+ \cdot 1HC$ (m/z 277) + CH_3OH	$\Delta H = 1.13$ eV (109.0 kJ/mol)	(6b)

$\rightarrow$ HG-9MG·[1HC + H$_{O2'}$]$^+$ (m/z 277) + CH$_3$OH ΔH = 1.35 eV (130.3 kJ/mol)   (6c)

$\rightarrow$ HG-9HG·[1MC + H$_{N3'}$]$^+$ (m/z 277) + CH$_3$OH ΔH = 1.06 eV (102.3 kJ/mol)   (6d)

$\rightarrow$ HG-[9HG + H$_{N7}$]$^+$·1MC (m/z 277) + CH$_3$OH ΔH = 1.19 eV (114.8 kJ/mol)   (6e)

$\rightarrow$ HG-9HG·[1MC + H$_{O2'}$]$^+$ (m/z 277) + CH$_3$OH ΔH = 1.39 eV (134.1 kJ/mol)   (6f)

$\rightarrow$ [1HC + H$_{N3'}$]$^+$ (m/z 112) + 9MG + CH$_3$OH ΔH = 2.98 eV (287.5 kJ/mol)   (7a)

$\rightarrow$ [9MG + H$_{N7}$]$^+$ (m/z 166) + 1HC + CH$_3$OH ΔH = 2.79 eV (269.2 kJ/mol)   (7b)

$\rightarrow$ [1HC + H$_{O2'}$]$^+$ (m/z 112) + 9MG + CH$_3$OH ΔH = 2.91 eV (280.8 kJ/mol)   (7c)

$\rightarrow$ [1MC + H$_{N3'}$]$^+$ (m/z 126) + 9HG + CH$_3$OH ΔH = 2.85 eV (275.0 kJ/mol)   (7d)

$\rightarrow$ [9HG + H$_{N7}$]$^+$ (m/z 152) + 1MC + CH$_3$OH ΔH = 3.00 eV (289.5 kJ/mol)   (7e)

$\rightarrow$ [1MC + H$_{O2'}$]$^+$ (m/z 126) + 9HG + CH$_3$OH ΔH = 2.80 eV (270.2 kJ/mol)   (7f)

Cross sections for individual product m/z are plotted as a function of E_{col} in Figs. 5b – e. The products

of m/z 112, 144, 152, 158, 184, 190 and 277 are all originated from the methanol elimination reactions, so

their intensities are lumped into Fig. 5e. Because each cross section has combined the contributions from

different product ion structures of the same m/z (and their secondary products), we were not able to

determine individual reaction thresholds. The cross section measurement has shown that, at low collision

energies, water ligand elimination [i.e., reactions (3a – c)] dominates over the other products. The

formation of [9MG + H]$^+$ and [1MC + H]$^+$ starts to emerge around 1.5 eV, becoming dominant above 4.0 eV.

The E_{col}-dependent branching ratio of $\frac{[1MC\ +\ H]^+}{[9MG\ +\ H]^+}$ is illustrated in Fig. 5f. The resemblance between the

$\frac{[1MC\ +\ H]^+}{[9MG\ +\ H]^+}$ detected in the CID of monohydrated base pair vs. that in the CID of dry base pair (see Fig. 2d)

implies that the dissociation of the HG base pair is governed by similar kinetics regardless of hydration.

3.3.2 Effects of Hydration on Reaction PES

Fig. 6a demonstrates the influence of hydration on the base-pair reactions. The species labeled in

bold are those that may be detected in the CID mass spectra. Reaction energetics were calculated at

different levels of theory and are compared in Table 3, of which the DLPNO-CCSD(T) values serve as

benchmark. The PT and dissociation reactions in HG-9MG·[1MC + H$_{N3'}$]$^+$·H$_2$O present identical

mechanisms, and similar activation energies and product enthalpies as the same type of reactions in dry

9MG·[1MC + H$_{N3'}$]$^+$. However, water ligand elimination and the accompanying product recoil energy

have consumed most of the excitation energy in HG-9MG·[1MC + $H_{N3'}$]$^+$, rendering the base pair itself being much less dissociative.

Fig. 6b maps out the reaction mechanism for a collision-induced chemical reaction between the N1′-methyl group in 1MC and the water ligand. The reaction is initiated by a second-order nucleophilic substitution (S_N2).[105, 106] The departure of the methyl from N1′ and the attack of water O atom on the methyl happen simultaneously. Subsequently, one of the water H atoms is transferred to the N1′ position. The ensuring HG-9MG·[1HC + $H_{N3'}$]$^+$ continues intra-base-pair PT to form HG-[9MG + H_{N7}]$^+$·1HC and HG-9MG·[1HC + $H_{O2'}$]$^+$, followed by the dissociations of the three base-pair conformers to [9MG + H]$^+$ and [1HC + H]$^+$ product ions. A similar methanol elimination reaction may occur at the N9-methyl of 9MG, as illustrated in Fig. 6c. We could not distinguish the two methanol-elimination pathways on the basis of product ion mass spectra. Considering that methanol elimination was also observed in the CID of [9MG·9MG + H]$^+$·H_2O and [1MC·1MC + H]$^+$·H_2O, it is most likely that both 9MG and 1MC have participated in methanol elimination. Note that all methanol elimination pathways involve high activation barriers (> 365 kJ/mol). However, the cross section of the product ions resulting from methanol elimination (Fig. 5e) has shown an appearance energy which is comparable to that of water ligand elimination (Fig. 5b). This leads us to attribute methanol elimination to the secondary reactions between dry base pair product ions and the dissociating water ligand. The same type of methanol elimination reaction was observed in the CID of WC-[9MG·1MC + H]$^+$·H_2O.[18]

Finally, we measured the CID of HG-9MG·[1MC + $H_{N3'}$]$^+$·H_2O with Ar gas. The collisions resulted in only [9MG·1MC + H]$^+$, [9MG·1HC + H]$^+$, [9HG·1MC + H]$^+$, [9MG + H]$^+$ and [1MC + H]$^+$ product ions. Compared to those in the Xe CID, the same reactions have presented higher appearance energies and lower cross sections in the Ar CID.

4. Conclusions

HG guanine–cytosine base pair expands the structural and functional versatility of the DNA duplex beyond that can be realized based on the WC base pair. The intra-base-pair PT and dissociation of HG

guanine–cytosine base pair have also inspired interest in reaction kinetics and dynamics, as the product distributions could not be rationalized using only static reaction minima and TSs. In the present work, HG-9MG·[1MC + $H_{N3'}$]$^+$ and its monohydrate were examined by measurement of E_{col}-resolved, HG isomer-specific CID reactions and computation of reaction PESs and unimolecular kinetics. The synergistic results have revealed various intra-base-pair PTs that lead to the formation of HG-9MG·[1MC + $H_{N3'}$]$^+$ > HG-[9MG + H_{N7}]$^+$·1MC >> HG-9MG·[1MC + $H_{O2'}$]$^+$, in the order of abundance. Surprisingly, despite HG-9MG·[1MC + $H_{O2'}$]$^+$ having the lowest population, it presents the highest dissociation rate constant which renders its dissociation product ion [1MC + $H_{O2'}$]$^+$ dominant over [9MG + H]$^+$ in the base-pair CID, both in the absence and presence of a water ligand.

The present work has resolved the previously reported "anomalies" in the dissociation product ion distributions of HG guanine-cytosine base pair. Our data analysis has suggested that the HG base-pair dissociation falls within the statistical kinetics regime. The contrasting difference between the statistical reaction behavior of the HG base pair and the non-statistical kinetics of its WC-isomer may be attributed to their different intra-base-pair H-bonds. Especially, the H bond between the N1 of 9MG and the N3′ of 1MC, which is responsible for the fast dissociation of a PT conformer in the WC base pair, is missing in the HG base pair.

Acknowledgement

Supporting Information

Cartesian coordinates for the structures in Figs. 1, 4 and 6, and description of loose TSs.

References
1   P. O. Löwdin, *Rev. Mod. Phys.*, 1963, **35**, 724-732, discussion 732-723.
2   L.-Y. Fu, G.-Z. Wang, B.-G. Ma and H.-Y. Zhang, *Biochem. Biophys. Res. Commun.*, 2011, **409**, 367-371.
3   J. Bertran, A. Oliva, L. Rodriguez-Santiago and M. Sodupe, *J. Am. Chem. Soc.*, 1998, **120**, 8159-8167.
4   L. Gorb, Y. Podolyan, P. Dziekonski, W. A. Sokalski and J. Leszczynski, *J. Am. Chem. Soc.*, 2004, **126**, 10119-10129.

5   Y. Lin, H. Wang, S. Gao, R. Li and H. F. Schaefer, III, *J. Phys. Chem. B*, 2012, **116**, 8908-8915.

6   V. Sauri, J. P. Gobbo, J. J. Serrano-Pérez, M. Lundberg, P. B. Coto, L. Serrano-Andrés, A. C. Borin, R. Lindh, M. Merchán and D. Roca-Sanjuán, *J. Chem. Theory Comput.*, 2013, **9**, 481-496.

7   E. E. Romero and F. E. Hernandez, *Phys. Chem. Chem. Phys.*, 2018, **20**, 1198-1209.

8   A. A. Arabi and C. F. Matta, *J. Phys. Chem. B*, 2018, **122**, 8631-8641.

9   G. P. Ford and B. Wang, *Int. J. Quantum Chem.*, 1992, **44**, 587-603.

10 M. Noguera, M. Sodupe and J. Bertrán, *Theor. Chem. Acc.*, 2004, **112**, 318-326.

11 S. Y. Han, S. H. Lee, J. Chung and H. B. Oh, *J. Chem. Phys.*, 2007, **127**, 245102.

12 Y. Lin, H. Wang, S. Gao and H. F. Schaefer, III, *J. Phys. Chem. B*, 2011, **115**, 11746–11756.

13 Y. Seong, S. Y. Han, S.-C. Jo and H. B. Oh, *Mass Spectrom. Lett.*, 2011, **2**, 73-75.

14 Y. Lin, H. Wang, Y. Wu, S. Gao and H. F. Schaefer, III, *Phys. Chem. Chem. Phys.*, 2014, **16**, 6717-6725.

15 A. F. Cruz-Ortiz, M. Rossa, F. Berthias, M. Berdakin, P. Maitre and G. A. Pino, *J. Phys. Chem. Lett.*, 2017, **8**, 5501-5506.

16 J. Jun and S. Y. Han, *Theor. Chem. Acc.*, 2017, **136**, 1-10.

17 J. J. Park, C. S. Lee and S. Y. Han, *J. Am. Soc. Mass Spectrom.*, 2018, **29**, 2368-2379.

18 Y. Sun, M. M. Moe and J. Liu, *Phys. Chem. Chem. Phys.*, 2020, **22**, 24986-25000.

19 W. Lu and J. Liu, *Phys. Chem. Chem. Phys.*, 2016, **18**, 32222-32237.

20 J. Liu, *Phys. Chem. Chem. Phys.*, 2017, **19**, 30616-30626.

21 K. Hildenbrand and D. Schulte-Frohlinde, *Free Radical Res. Commun.*, 1990, **11**, 195-206.

22 A. O. Colson, B. Besler and M. D. Sevilla, *J. Phys. Chem.*, 1992, **96**, 9787-9794.

23 M. Hutter and T. Clark, *J. Am. Chem. Soc.*, 1996, **118**, 7574-7577.

24 E. Nir, K. Kleinermanns and M. S. de Vries, *Nature (London)*, 2000, **408**, 949-950.

25 X. Li, Z. Cai and M. D. Sevilla, *J. Phys. Chem. B*, 2001, **105**, 10115-10123.

26 K. Kobayashi and S. Tagawa, *J. Am. Chem. Soc.*, 2003, **125**, 10213-10218.

27 A. K. Ghosh and G. B. Schuster, *J. Am. Chem. Soc.*, 2006, **128**, 4172-4173.

28 K. Kobayashi, R. Yamagami and S. Tagawa, *J. Phys. Chem. B*, 2008, **112**, 10752-10757.

29 A. Kumar and M. D. Sevilla, *J. Phys. Chem. B*, 2009, **113**, 11359-11361.

30 A. W. Parker, C. Y. Lin, M. W. George, M. Towrie and M. K. Kuimova, *J. Phys. Chem. B*, 2010, **114**, 3660-3667.

31 J. P. Ceron-Carrasco, A. Requena, E. A. Perpete, C. Michaux and D. Jacquemin, *J. Phys. Chem. B*, 2010, **114**, 13439-13445.

32 S. Steenken and J. Reynisson, *Phys. Chem. Chem. Phys.*, 2010, **12**, 9088-9093.

33 Y. Rokhlenko, J. Cadet, N. E. Geacintov and V. Shafirovich, *J. Am. Chem. Soc.*, 2014, **136**, 5956-5962.

34 A. Kumar and M. D. Sevilla, *J. Phys. Chem. B*, 2014, **118**, 5453-5458.

35 J. Jie, K. Liu, L. Wu, H. Zhao, D. Song and H. Su, *Sci. Adv.*, 2017, **3**, e1700171.

36 L. Feketeová, B. Chan, G. N. Khairallah, V. Steinmetz, P. Maitre, L. Radom and R. A. J. O'Hair, *J. Phys. Chem. Lett.*, 2017, **8**, 3159-3165.

37 Y. Sun, M. M. Moe and J. Liu, *Phys. Chem. Chem. Phys.*, 2020, **20**, 14875-14888.

38 H.-Y. Chen, C.-L. Kao and S. C. N. Hsu, *J. Am. Chem. Soc.*, 2009, **131**, 15930-15938.

39 A. Szyperska, J. Rak, J. Leszczynski, X. Li, Y. J. Ko, H. Wang and K. H. Bowen, *ChemPhysChem*, 2010, **11**, 880-888.

40 H.-Y. Chen, S.-W. Yeh, S. C. N. Hsu, C.-L. Kao and T.-Y. Dong, *Phys. Chem. Chem. Phys.*, 2011, **13**, 2674-2681.

41 A. Gupta, H. M. Jaeger, K. R. Compaan and H. F. Schaefer, III, *J. Phys. Chem. B*, 2012, **116**, 5579-5587.

42 J. Gu, J. Wang and J. Leszczynski, *J. Phys. Chem. B*, 2015, **119**, 2454-2458.

43 J. D. Zhang, Z. Chen and H. F. Schaefer, III, *J. Phys. Chem. A*, 2008, **112**, 6217-6226.

44 Y. Han and D. Li, *J. Mol. Model*, 2019, **25**, 40.

45 J. D. Watson and F. H. C. Crick, *Nature*, 1953, **171**, 737-738.

46 C. Colominas, F. J. Luque and M. Orozco, *J. Am. Chem. Soc.*, 1996, **118**, 6811-6821.
47 C. I. Morari and C. M. Muntean, *Biopolymers*, 2003, **72**, 339-344.
48 H. Wang, J. D. Zhang and H. F. Schaefer, III, *ChemPhysChem*, 2010, **11**, 622-629.
49 Y. M. Petrenko, *Biophysics (Engl. Transl.)*, 2015, **60**, 701-707.
50 K. Hoogsteen, *Acta Crystallogr.*, 1959, **12**, 822-823.
51 K. Hoogsteen, *Acta Crystallogr.*, 1963, **16**, 907-916.
52 Y. Courtois, P. Fromageot and W. Guschlbauer, *Eur. J. Biochem.*, 1968, **6**, 493-501.
53 G. J. Quigley, G. Ughetto, G. A. Van der Marel, J. H. Van Boom, A. H. J. Wang and A. Rich, *Science*, 1986, **232**, 1255-1258.
54 E. N. Nikolova, H. Zhou, F. L. Gottardo, H. S. Alvey, I. J. Kimsey and H. M. Al-Hashimi, *Biopolymers*, 2013, **99**, 955-968.
55 E. N. Nikolova, E. Kim, A. A. Wise, P. J. O'Brien, I. Andricioaei and H. M. Al-Hashimi, *Nature*, 2011, **470**, 498-502.
56 E. N. Nikolova, F. L. Gottardo and H. M. Al-Hashimi, *J. Am. Chem. Soc.*, 2012, **134**, 3667-3670.
57 H. S. Alvey, F. L. Gottardo, E. N. Nikolova and H. M. Al-Hashimi, *Nat. Commun.*, 2014, **5**, 4786.
58 D. Coman and I. Russu, *J. Biol. Chem.*, 2005, **280**, 20216-20221.
59 G. J. Puppels, C. Otto, J. Greve, M. Robert-Nicoud, D. J. Arndt-Jovin and T. M. Jovin, *Biochem.*, 1994, **33**, 3386-3395.
60 B. L. Haas and W. Guschlbauer, *Nucleic Acids Res.*, 1976, **3**, 205-218.
61 G. A. Patikoglou, J. L. Kim, L. Sun, S.-H. Yang, T. Kodadek and S. K. Burley, *Genes Dev.*, 1999, **13**, 3217-3230.
62 M. W. Kalnik, B. F. L. Li, P. F. Swann and D. J. Patel, *Biochem.*, 1989, **28**, 6182-6192.
63 D. T. Nair, R. E. Johnson, S. Prakash, L. Prakash and A. K. Aggarwal, *Nature*, 2004, **430**, 377-380.
64 D. T. Nair, R. E. Johnson, L. Prakash, S. Prakash and A. K. Aggarwal, *Structure*, 2005, **13**, 1569-1577.
65 J. J. Park and S. Y. Han, *J. Am. Soc. Mass Spectrom.*, 2019, **30**, 846-854.
66 R. Cheng, J. Martens and T. D. Fridgen, *Phys. Chem. Chem. Phys.*, 2020, **22**, 11546-11557.
67 Y. Fang and J. Liu, *J. Phys. Chem. A*, 2009, **113**, 11250-11261.
68 C. Rebick and R. D. Levine, *J. Chem. Phys.*, 1973, **58**, 3942-3952.
69 R. D. Levine and R. B. Bernstein, *Molecular Reaction Dynamics and Chemical Reactivity*, Oxford University Press, New York, 1987.
70 P. B. Armentrout, *Int. J. Mass Spectrom.*, 2000, **200**, 219-241.
71 J. Liu, B. van Devener and S. L. Anderson, *J. Chem. Phys.*, 2002, **116**, 5530-5543.
72 M. B. Sowa-Resat, P. A. Hintz and S. L. Anderson, *J. Phys. Chem.*, 1995, **99**, 10736-10741.
73 M. T. Rodgers, K. M. Ervin and P. B. Armentrout, *J. Chem. Phys.*, 1997, **106**, 4499-4508.
74 R. A. Marcus, *J. Chem. Phys.*, 1952, **20**, 359-364.
75 M. J. Frisch, G. W. Trucks, H. B. Schlegel, G. E. Scuseria, M. A. Robb, J. R. Cheeseman, G. Scalmani, V. Barone, B. Mennucci, G. A. Petersson, H. Nakatsuji, M. Caricato, X. Li, H. P. Hratchian, A. F. Izmaylov, J. Bloino, G. Zheng, J. L. Sonnenberg, M. Hada, M. Ehara, K. Toyota, R. Fukuda, J. Hasegawa, M. Ishida, T. Nakajima, Y. Honda, O. Kitao, H. Nakai, T. Vreven, J. J. A. Montgomery, J. E. Peralta, F. Ogliaro, M. Bearpark, J. J. Heyd, E. Brothers, K. N. Kudin, V. N. Staroverov, T. Keith, R. Kobayashi, J. Normand, K. Raghavachari, A. Rendell, J. C. Burant, S. S. Iyengar, J. Tomasi, M. Cossi, N. Rega, J. M. Millam, M. Klene, J. E. Knox, J. B. Cross, V. Bakken, C. Adamo, J. Jaramillo, R. Gomperts, R. E. Stratmann, O. Yazyev, A. J. Austin, R. Cammi, C. Pomelli, J. W. Ochterski, R. L. Martin, K. Morokuma, V. G. Zakrzewski, G. A. Voth, P. Salvador, J. J. Dannenberg, S. Dapprich, A. D. Daniels, O. Farkas, J. B. Foresman, J. V. Ortiz, J. Cioslowski and D. J. Fox, Gaussian 09, Rev. D.01, Gaussian, Inc, Wallingford, CT, 2013.
76 J.-D. Chai and M. Head-Gordon, *Phys. Chem. Chem. Phys.*, 2008, **10**, 6615-6620.
77 F. B. van Duijneveldt, J. G. C. M. van Duijneveldt-van de Rijdt and J. H. van Lenthe, *Chem. Rev.*, 1994, **94**, 1873-1885.
78 F. Weigend, M. Haser, H. Patzelt and R. Ahlrichs, *Chem. Phys. Lett.*, 1998, **294**, 143-152.

79 P. Jurecka, P. Nachtigall and P. Hobza, *Phys. Chem. Chem. Phys.*, 2001, **3**, 4578-4582.
80 D. G. Liakos, M. Sparta, M. K. Kesharwani, J. M. L. Martin and F. Neese, *J. Chem. Theory Comput.*, 2015, **11**, 1525-1539.
81 F. Neese, *WIREs Comput Mol Sci*, 2018, **8**, e1327.
82 I. M. Alecu, J. Zheng, Y. Zhao and D. G. Truhlar, *J. Chem. Theory Comput.*, 2010, **6**, 2872-2887.
83 T. Baer and W. L. Hase, *Unimolecular reaction dynamics: Theory and experiments*, Oxford University Press, New York, 1996.
84 W. L. Hase, *Acc. Chem. Res.*, 1998, **31**, 659-665.
85 K. Fukui, *J. Phys. Chem.*, 1970, **74**, 461-463.
86 L. Zhu and W. L. Hase, A General RRKM Program (QCPE 644), Quantum Chemistry Program Exchange, Chemistry Department, University of Indiana, Bloomington, 1993.
87 T. Beyer and D. F. Swinehart, *Commun. ACM*, 1973, **16**, 379.
88 L. Zhu and W. L. Hase, *Chem. Phys. Lett.*, 1990, **175**, 117-124.
89 J. Bordas-Nagy and K. R. Jennings, *Int. J. Mass Spectrom. Ion Processes*, 1990, **100**, 105-131.
90 P. B. Armentrout, *J. Am. Soc. Mass Spectrom.*, 2002, **13**, 419-434.
91 P. B. Armentrout, *J. Anal. At. Spectrom.*, 2004, **19**, 571-580.
92 J. Liu, B. Uselman, J. Boyle and S. L. Anderson, *J. Chem. Phys.*, 2006, **125**, 133115.
93 E. Wigner, *Z. physik. Chem.*, 1932, **B19**, 203-216.
94 A. Martin-Somer, R. Spezia and M. Yanez, *Philos. Trans. R. Soc., A*, 2017, **375**, 20160196/20160191-20160196/20160117.
95 F. Meyer, F. A. Khan and P. B. Armentrout, *J. Am. Chem. Soc.*, 1995, **117**, 9740-9748.
96 M. B. More, E. D. Glendening, D. Ray, D. Feller and P. B. Armentrout, *J. Phys. Chem.*, 1996, **100**, 1605-1614.
97 D. Ray, D. Feller, M. B. More, E. D. Glendening and P. B. Armentrout, *J. Phys. Chem.*, 1996, **100**, 16116-16125.
98 M. T. Rodgers and P. B. Armentrout, *J. Chem. Phys.*, 1998, **109**, 1787-1800.
99 S. J. Klippenstein, A. L. L. East and W. D. Allen, *J. Chem. Phys.*, 1994, **101**, 9198-9201.
100 P. C. Haarhoff, *Mol. Phys.*, 1964, **7**, 101-117.
101 J. Troe, *Chem. Phys. Lett.*, 1985, **122**, 425-430.
102 P. Langevin, *Ann. Chim. Phys.*, 1905, **5**, 245-288.
103 L. P. Theard and W. H. Hamill, *J. Am. Chem. Soc.*, 1962, **84**, 1134-1139.
104 S. K. Gupta, E. G. Jones, A. G. Harrison and J. J. Myher, *Can. J. Chem.*, 1967, **45**, 3107-3117.
105 J. K. Laerdahl and E. Uggerud, *Int. J. Mass Spectrom.*, 2002, **214**, 277-314.
106 E. Uggerud, *Pure Appl. Chem.*, 2009, **81**, 709-717.

Table 1   Comparison of reaction enthalpies (298 K, eV) of HG-9MG·[1MC + H$_{N3'}$]$^+$·1MC at different levels of
theory

species	ωB97XD/ 6-311++G(d,p)	ωB97XD/ aug-cc-pVQZ	B3LYP/ aug-cc-pVQZ	RI-MP2/ aug-cc-pVTZ	DLPNO-CCSD(T)/ aug-cc-pVTZ
HG-9MG·[1MC + H$_{N3'}$]$^+$	0.00	0.00	0.00	0.00	0.00
9MG + [1MC + H$_{N3'}$]$^+$	1.91	1.85	1.70	1.93	1.86
TS_PT3′	0.03	0.05	0.05	0.01	0.05
HG-[9MG + H$_{N7}$]$^+$·1MC	0.10	0.11	0.11	0.10	0.11
[9MG + H$_{N7}$]$^+$ + 1MC	1.86	1.78	1.61	1.88	1.82
TS_PT7	0.35	0.32	0.29	0.24	0.27
HG-9MG·[1MC + H$_{O2'}$]$^+$	0.43	0.39	0.38	0.31	0.32
9MG + [1MC + H$_{O2'}$]$^+$	1.95	1.87	1.72	1.88	1.81

Table 2   Relative populations of three different HG base-pair conformers formed in collisional activation and their product ion branching ratios predicted by tight- and loose-TS-RRKM

E_{col}	HG-9MG·$[1MC + H_{N3'}]^+$: HG-$[9MG + H_{N7}]^+$·1MC : HG-9MG·$[1MC + H_{O2'}]^+$	$[1MC + H_{N3'}]^+$: $[9MG + H_{N7}]^+$: $[1MC + H_{O2'}]^+$	
		tight-TS-RRKM	loose-TS-RRKM
2.2	0.69 : 0.30 : 0.01	0.03 : 0.40 : 0.57	0.02 : 0.20 : 0.78
2.4	0.67 : 0.32 : 0.01	0.05 : 0.43 : 0.52	0.03 : 0.21 : 0.76
2.6	0.65 : 0.34 : 0.01	0.06 : 0.44 : 0.50	0.04 : 0.23 : 0.73
2.8	0.63 : 0.36 : 0.01	0.07 : 0.45 : 0.48	0.05 : 0.24 : 0.71
3.0	0.61 : 0.38 : 0.01	0.07 : 0.46 : 0.47	0.06 : 0.25 : 0.69
3.2	0.59 : 0.39 : 0.02	0.08 : 0.46 : 0.46	0.08 : 0.26 : 0.66
3.4	0.57 : 0.41 : 0.02	0.08 : 0.47 : 0.45	0.09 : 0.26 : 0.65
3.6	0.56 : 0.42 : 0.02	0.09 : 0.47 : 0.44	0.10 : 0.27 : 0.63
3.8	0.54 : 0.43 : 0.03	0.09 : 0.48 : 0.43	0.10 : 0.27 : 0.63
4.0	0.53 : 0.44 : 0.03	0.09 : 0.48 : 0.43	0.11 : 0.27: 0.62
4.2	0.52 : 0.45 : 0.03	0.10 : 0.48 : 0.42	0.11 : 0.28 : 0.61

Table 3 Comparison of reaction enthalpies (298 K, eV) of HG-9MG·[1MC + H$_{N3'}$]$^+$·H$_2$O at different levels of theory

species	ωB97XD/ 6-311++G(d,p)	ωB97XD/ aug-cc-pVQZ	B3LYP/ aug-cc-pVQZ	RI-MP2/ aug-cc-pVTZ	DLPNO-CCSD(T)/ aug-cc-pVTZ
HG-9MG·[1MC + H$_{N3'}$]$^+$·H$_2$O	0.00	0.00	0.00	0.00	0.00
HG-9MG·[1MC + H$_{N3'}$]$^+$ + H$_2$O	0.55	0.46	0.39	0.49	0.47
9MG + [1MC + H$_{N3'}$]$^+$ + H$_2$O	2.46	2.31	2.09	2.43	2.33
TS_PT3′·H$_2$O	0.01	0.03	0.03	-0.02	0.02
HG-[9MG + H$_{N7}$]$^+$·1MC·H$_2$O	0.07	0.08	0.08	0.06	0.07
HG-[9MG + H$_{N7}$]$^+$·1MC + H$_2$O	0.65	0.57	0.51	0.59	0.58
[9MG + H$_{N7}$]$^+$ + 1MC + H$_2$O	2.41	2.24	2.00	2.37	2.29
TS_PT7·H$_2$O	0.37	0.35	0.32	0.26	0.29
HG-9MG·[1MC + H$_{O2'}$]$^+$·H$_2$O	0.46	0.42	0.40	0.34	0.35
HG-9MG·[1MC + H$_{O2'}$]$^+$ + H$_2$O	0.98	0.86	0.77	0.81	0.79
9MG + [1MC + H$_{O2'}$]$^+$ + H$_2$O	2.50	2.34	2.11	2.37	2.28
TS1	3.72	3.77	3.51	3.89	3.78
HG-9MG·[1HC + H$_{N3'}$]$^+$ + CH$_3$OH	1.06	0.96	0.81	1.15	1.04
9MG + [1HC + H$_{N3'}$]$^+$ + CH$_3$OH	3.04	2.89	2.59	3.17	2.98
TS1_PT3′	1.08	1.00	0.84	1.15	1.08
HG-[9MG + H$_{N7}$]$^+$·1HC + CH$_3$OH	1.15	1.05	0.90	1.24	1.13
[9MG + H$_{N7}$]$^+$ + 1HC + CH$_3$OH	2.85	2.67	2.35	2.97	2.79
TS1_PT7	1.40	1.27	1.08	1.38	1.29
HG-9MG·[1HC + H$_{O2'}$]$^+$ + CH$_3$OH	1.48	1.34	1.17	1.46	1.35
9MG + [1HC + H$_{O2'}$]$^+$ + CH$_3$OH	3.07	2.88	2.59	3.09	2.91
TS2	3.92	3.97	3.72	4.01	3.93
HG-9HG·[1MC + H$_{N3'}$]$^+$ + CH$_3$OH	1.09	0.99	0.84	1.19	1.06
9HG + [1MC + H$_{N3'}$]$^+$ + CH$_3$OH	2.94	2.78	2.48	3.05	2.85
TS2_PT3′	1.17	1.07	0.93	1.24	1.15
HG-[9HG + H$_{N7}$]$^+$·1MC + CH$_3$OH	1.22	1.11	0.97	1.30	1.19
[9HG + H$_{N7}$]$^+$ + 1MC + CH$_3$OH	3.07	2.88	2.56	3.17	3.00
TS2_PT7	1.47	1.33	1.16	1.46	1.36
HG-9HG·[1MC + H$_{O2'}$]$^+$ + CH$_3$OH	1.53	1.39	1.22	1.51	1.39
9HG + [1MC + H$_{O2'}$]$^+$ + CH$_3$OH	2.98	2.80	2.50	2.99	2.90

Scheme 1 Watson-Crick and Hoogsteen structures of [9MG·1MC + H]$^+$, presented with atomic numbering scheme and possible intra-base-pair PT pathways

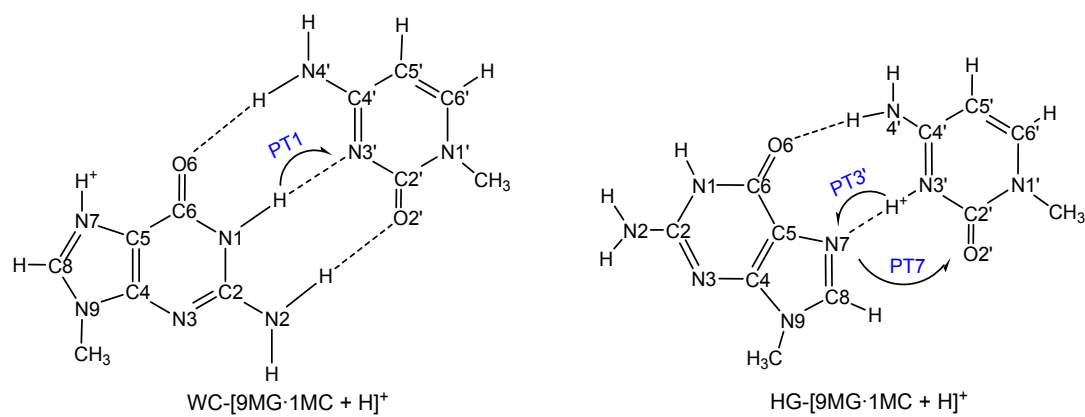WC-[9MG·1MC + H]$^+$ HG-[9MG·1MC + H]$^+$

Figure Caption

Fig. 1   Stable conformers of HG-[9MG·1MC + H]$^+$·(H$_2$O)$_{0,1}$. Dashed lines indicate H-bonds with bond

lengths shown in Å. Relative enthalpies (ΔH with respect to the global minimum, eV) and

hydration enthalpies (ΔH$_{hydration}$, eV) at 298 K were calculated at the ωB97XD/6-311++G(d,p)

level of theory, including thermal corrections.

Fig. 2   CID results of HG-9MG·[1MC + H$_{N3'}$]$^+$ with Xe: (a) product ion mass spectrum measured at E_{col}

= 3.0 eV; (b, c) individual product ion cross sections as a function of E_{col}, where circled points are

experimental data and blue-colored lines are LOC fits as described in the text, and (d) branching

ratio of $\frac{[1MC + H]^+}{[9MG + H]^+}$ as a function of E_{col}.

Fig. 3   CID results of HG-9MG·[1MC + H$_{N3'}$]$^+$ with Ar: (a, b) individual product ion cross sections and

(c) branching ratio of $\frac{[1MC + H]^+}{[9MG + H]^+}$ as a function of E_{col}.

Fig. 4   Schematic PES for intra-base-pair PT and dissociation of HG-9MG·[1MC + H$_{N3'}$]$^+$. Reaction

enthalpies were calculated at the DLPNO-CCSD(T)/aug-cc-pVTZ//ωB97XD/6-311++G(d,p)

levels of theory, including thermal corrections at 298 K.

Fig. 5   CID results of HG-9MG·[1MC + H$_{N3'}$]$^+$·H$_2$O with Xe: (a) product ion mass spectrum measured

at E_{col} = 3.0 eV; (b – d) individual product ion cross sections, and (e) branching ratio of

$\frac{[1MC + H]^+}{[9MG + H]^+}$ as a function of E_{col}.

Fig. 6   Schematic PES for intra-base-pair PT, water and methanol elimination, and dissociation of HG-

9MG·[1MC + H$_{N3'}$]$^+$·H$_2$O. Reaction enthalpies were calculated at the DLPNO-CCSD(T)/aug-cc-

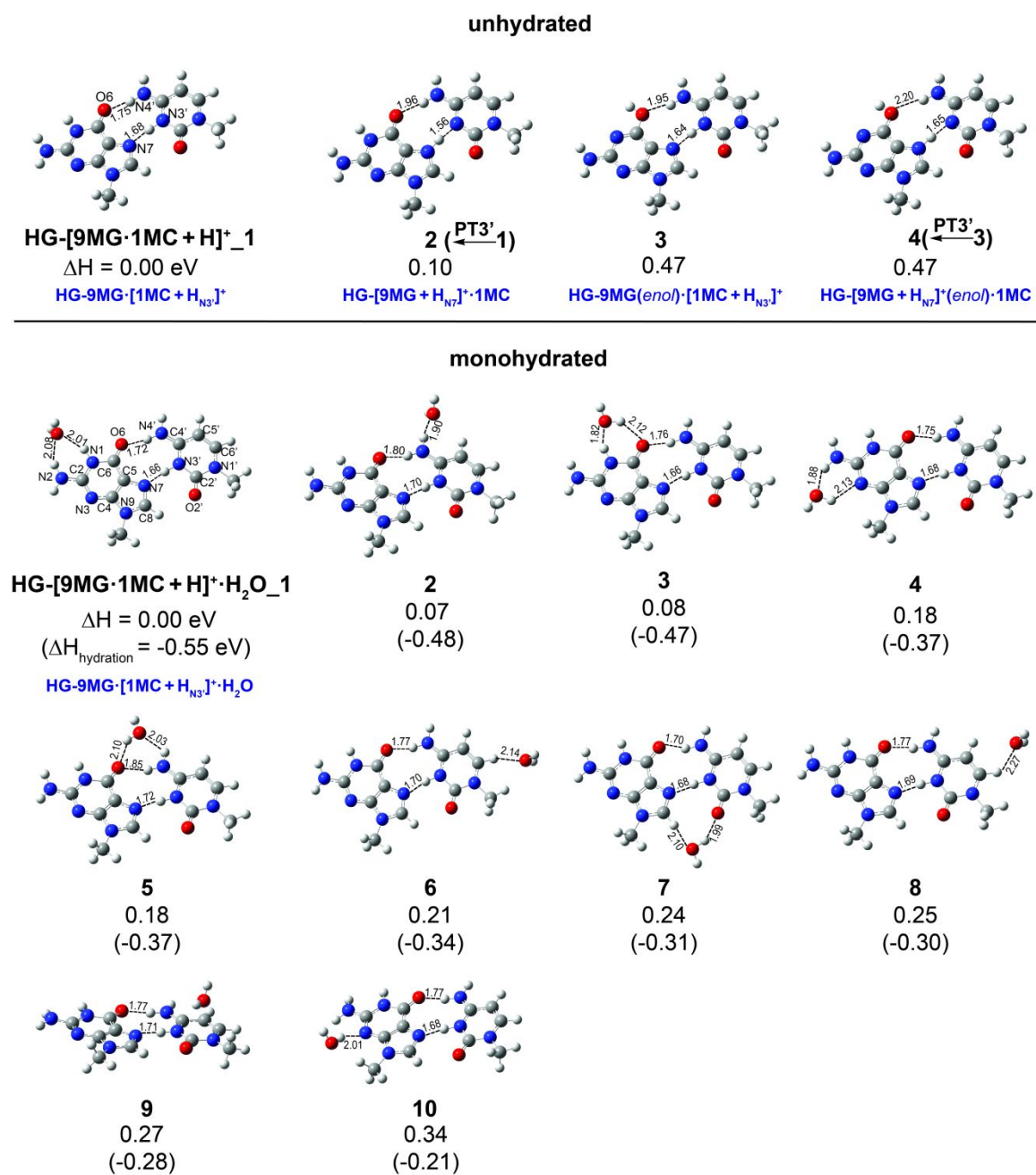pVTZ//ωB97XD/6-311++G(d,p) levels of theory, including thermal corrections at 298 K.

Fig. 1

unhydrated

HG-[9MG·1MC + H]⁺_1
ΔH = 0.00 eV
HG-9MG·[1MC + H$_{N3'}$]⁺

2 (← PT3' 1)
0.10
HG-[9MG + H$_{N7}$]⁺·1MC

3
0.47
HG-9MG(*enol*)·[1MC + H$_{N3'}$]⁺

4(← PT3' 3)
0.47
HG-[9MG + H$_{N7}$]⁺(*enol*)·1MC

monohydrated

HG-[9MG·1MC + H]⁺·H₂O_1
ΔH = 0.00 eV
(ΔH$_{hydration}$ = -0.55 eV)
HG-9MG·[1MC + H$_{N3'}$]⁺·H₂O

2
0.07
(-0.48)

3
0.08
(-0.47)

4
0.18
(-0.37)

5
0.18
(-0.37)

6
0.21
(-0.34)

7
0.24
(-0.31)

8
0.25
(-0.30)

9
0.27
(-0.28)

10
0.34
(-0.21)

Fig. 2

a) Xe CID [9MG·1MC + H]⁺ m/z 291

[1MC + H]⁺ 126

[9MG + H]⁺ 166

b) [9MG + H]⁺ $E_0 = 1.85$

c) [1MC + H]⁺ $E_0 = 1.90$

d) branching ratio
- Experimental
- Loose-TS-RRKM
- Tight-TS-RRKM

Fig. 3

Fig. 4

Fig. 5

a) Xe CID

b) Rxn 3

c) Rxn 4

d) Rxn 5

e) CH$_3$OH eli.

f) branching ratio

Fig. 6

36